Giant anisotropy of magnetic damping in an epitaxial Cr/Fe bilayer with the absence of magnetocrystalline anisotropy

Thanh-Huong Thi Nguyen [ID],[1] Jungmin Park [ID],[2] Jae-Hyun Ha [ID],[1] Soogil Lee,[3] Van Quang Nguyen [ID],[4] Nyun Jong Lee [ID],[5]
Byong-Guk Park [ID],[3] Sunglae Cho,[5] Jung-Il Hong [ID],[1,*] and Sanghoon Kim [ID][5,†]

[1]*Department of Physics and Chemistry, Daegu Gyeongbuk Institute of Science and Technology, Daegu 42988, Korea*
[2]*Department of Physics, Korea Advanced Institute of Science and Technology, Daejeon 34141, Korea*
[3]*Department of Materials Science and Engineering, Korea Advanced Institute of Science and Technology, Daejeon 34141, Korea*
[4]*Korea Atomic Energy Research Institute, Daejeon 34057, Korea*
[5]*Department of Physics, University of Ulsan, Ulsan 44610, Korea*

Magnetic damping is one of the most important parameters governing the critical current density for current-induced magnetization switching in spin-torque devices. The anisotropic nature of magnetic damping, influenced by both intrinsic and extrinsic factors, has been demonstrated in both theoretical and experimental studies. Nevertheless, understanding the underlying mechanisms of magnetic damping anisotropy, particularly in the bilayer structure of a ferromagnet and a nonmagnetic metal, remains an open challenge. In this study, we investigate the crystallographic dependence of magnetic damping in an epitaxial Cr/Fe bilayer, which has negligible magnetocrystalline anisotropy. We experimentally extracted the total damping by conducting frequency-dependent ferromagnetic resonance measurement at different in-plane angles. The observed damping reveals a strong angular dependence with an anisotropy of ~400% in the bilayer. All possible contributions to the total damping will be discussed carefully to clarify the origin of the profound damping anisotropy observed in our Cr/Fe bilayer.

Relaxation of the excited magnetic state to the equilibrium state, where magnetic energy dissipates into the surrounding medium, is a complex phenomenon making it an active topic in the field of spintronics. The rate of magnetic relaxation, also known as magnetic damping (α), is a crucial parameter for the efficient operation of various spin-based devices, such as magnetic random-access memories (MRAM), spin-torque oscillators, and magnonic circuits [1–4]. It has been theoretically suggested that α has an anisotropic nature rather than isotropic [5,6]. The origin of this anisotropy is diverse, with many factors potentially influencing magnetic damping. Recent experimental studies have shown that anisotropy of the Gilbert damping (α_G), which is an intrinsic character of ferromagnetic thin films, can be attributed to spatial variation in spin-orbit coupling at the interface with the substrate or within the crystal structure. For example, Chen *et al.* reported the twofold symmetry of α_G, which originates from the twofold symmetry of spin-orbit coupling at the Fe/GaAs interface [7]. Similarly, Li *et al.* reported a giant damping anisotropy of 440% in an epitaxial $Fe_{50}Co_{50}$ thin film, which is attributed to tetragonal crystal distortion [8]. Apart from the α_G, additional damping (α_{sp}) induced by spin pumping effect in the ferromagnet (FM)/nonmagnetic metal (NM) bilayer can also exhibit anisotropic behavior [9]. Furthermore, other extrinsic effects, such as two-magnon scattering, can

also contribute to the crystallographic dependence of magnetic damping [10,11]. From a practical point of view, the performance of magnetic devices may not be influenced solely by intrinsic damping α_G, but the total damping α_{tot}, which is a joint phenomenon from both intrinsic and extrinsic effects. Thus, each contribution should be thoroughly considered to understand the mechanisms behind the magnetic damping anisotropy in specific systems when designing magnetic devices and further optimizing magnetic device performance.

Motivated by these findings, our study reports the angular dependence of magnetic damping in an epitaxial Cr/Fe bilayer, although its magnetic anisotropy is found to be negligible. The Cr/Fe structure is widely recognized as a classical framework in the field of magnetism owing to its giant magnetoresistance [12–15]. Moreover, among 3*d* transition metals, Cr has been reported to exhibit a large orbital Hall conductivity originating from orbital texture in Cr, which is even larger than its spin Hall conductivity [16–18]. Though the Cr/Fe system has been one of the popular material systems in the spintronics field, there is still lack of experimental studies on the possible anisotropic damping in Cr/Fe bilayers. Therefore, it is desirable to investigate the angular dependence of the α_{tot} in the Cr/Fe bilayer. To experimentally calculate the α_{tot}, we performed frequency-dependent ferromagnetic resonance (FMR) measurements with respect to in-plane angles and observed a profound damping anisotropy in our bilayers. To interpret the FMR result, we carefully considered all possible intrinsic and extrinsic effects that contribute to the total damping in the Cr/Fe bilayer. Extrinsic effects are believed

---

*Corresponding author: jihong@dgist.ac.kr
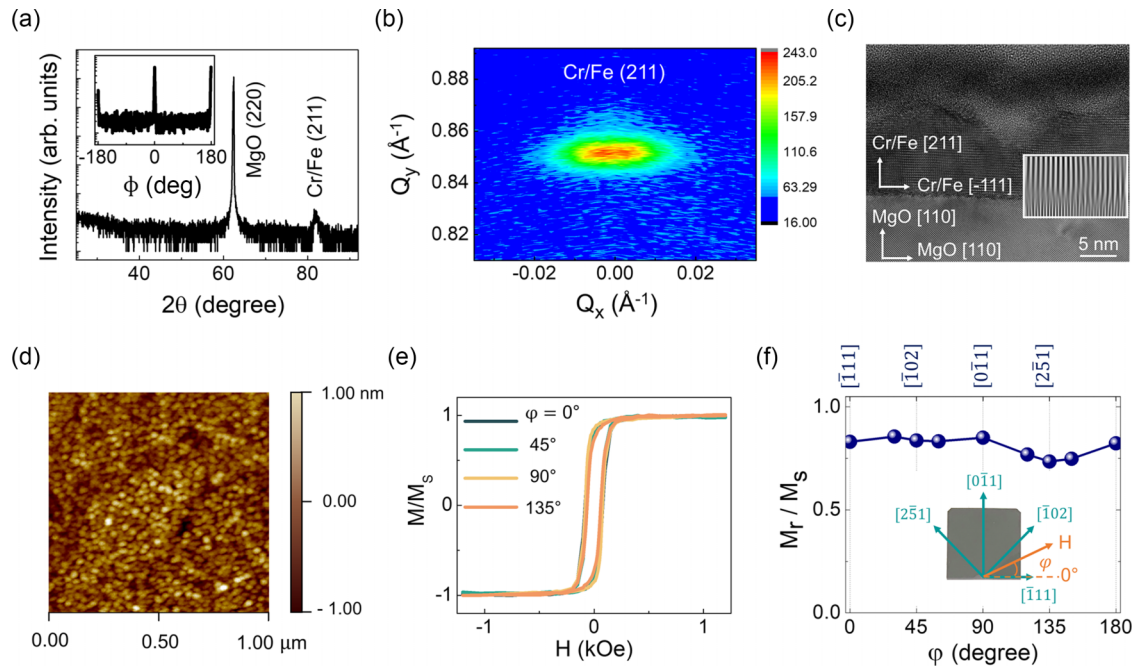†Corresponding author: sanghoon.kim@ulsan.ac.kr

FIG. 1. (a) θ-2θ x-ray diffraction pattern for the Cr/Fe film on MgO (110) substrate. Inset in (a) is ϕ scan (in-plane rotation scan) pattern of Cr/Fe (011). (b) Reciprocal space mapping taken around Cr/Fe (211) diffraction peak. (c) Cross-sectional high-resolution transmission electron microscopy (HR-TEM) image of the Cr/Fe bilayer film on MgO substrate with MgO (110) [001] zone axis. Inset in (c) is a Fourier filter image of the interface between MgO substrate and the subsequent Cr layer. (d) Atomic force microscopy (AFM) image of surface topography for Cr/Fe (211) film. (e) Normalized magnetization curve (M/M_S) of Cr/Fe (211) film where the external magnetic field applied along $\varphi = 0°$; $45°$; $90°$; $135°$. (f) Angular dependence of the ratio of remanent magnetization (M_r) to the saturation magnetization (M_S) obtained from in-plane hysteresis loops at various φ. Inset in (f) is an image of the Cr/Fe film on MgO (110) substrate with the blue arrows indicating crystal directions. The orange arrow indicates the in-plane external magnetic field direction. The azimuthal angle labeled by φ is defined as the angle between the external magnetic field H and the [-111] crystal direction.

to dominantly contribute to the α_{tot} in our Cr/Fe bilayer. Presumably, the most relevant effect would associate the angular momentum dissipation with the orbital texture of Cr, which shows strong crystallographic dependence.

The Cr (5 nm)/Fe (4 nm) bilayers were successfully grown by molecular beam epitaxy (MBE) method. The MgO (110) substrates were first annealed at $\sim 680\,°C$ for 15 min to remove residual organic contaminations. Afterwards the Cr and Fe layers were grown at the growth temperatures T_{growth} of $\sim 400\,°C$ and $\sim 150°C$, respectively, under a base pressure of $\sim 10^{-9}$ Torr. Finally, the capping layer of Mg (1 nm) / MgO$_x$ (2 nm) was deposited to prevent oxidation in the ambient condition. The crystalline structure of the Cr/Fe bilayer were examined using a high-resolution transmission emission microscope (HR-TEM) and reciprocal space mapping (RSM) was carried out with x-ray diffraction. Static magnetic property was then characterized by conducting a vibration sample measurement. During the measurement, the external magnetic field was applied along different azimuthal directions (φ) within the film plane.

The broadband ferromagnetic resonance measurement (FMR) was carried out by mounting the samples surface down on the coplanar waveguide, which was connected to a microwave source. The microwave current (I_{rf}) was fixed at the power of ~ 15 dBm and microwave frequency spanning from 10 GHz to 19 GHz, while the external magnetic field was sweeping parallel to the I_{rf}. A lock-in amplifier was used to detect the derivative of the microwave absorption in terms of

the external magnetic field. The crystallographic dependence of FMR spectra were investigated by applying the external magnetic field at different crystal directions. All FMR measurements were conducted at room temperature. For the spin Hall magnetoresistance (SMR) and anisotropic magnetoresistance (AMR) measurements, the single Hall-bar devices were fabricated with the current line along different crystallographic orientations using ion milling and photolithography process.

The crystallinity of the Cr/Fe film on MgO (110) substrate was examined by x-ray diffraction (XRD) as shown in Figs. 1(a) and 1(b). As clearly seen from the θ-2θ scan result, the single phase of the Cr/Fe (211) peak was solely observed without additional peaks [see Fig. 1(a)]. Moreover, the ϕ scan result shown in the inset of Fig. 1(a) reveals a typical twofold symmetry of the tetragonal crystal of Cr/Fe (211) [12]. Figure 1(b) shows the RSM around the (211) diffraction peak. The peak is elongated along [-111] direction, thus revealing the presence of strain due to a lattice misfit between MgO and Cr ($\sim 17\%$) [19].

The crystal structure of the Cr/Fe film was visualized by a cross-sectional transmission electron microscopy (TEM) as shown in Fig. 1(c). We can confirm the in-plane epitaxial relation between Cr/Fe (211) film and MgO (110) : Cr/Fe (211) [-111] // MgO (110) [-110] from the TEM image. The Fourier-filtered image [inset of Fig. 1(c)] shows misfit dislocations periodically introduced at the MgO/Cr interface to relax the 17% lattice misfit. Despite the presence of the
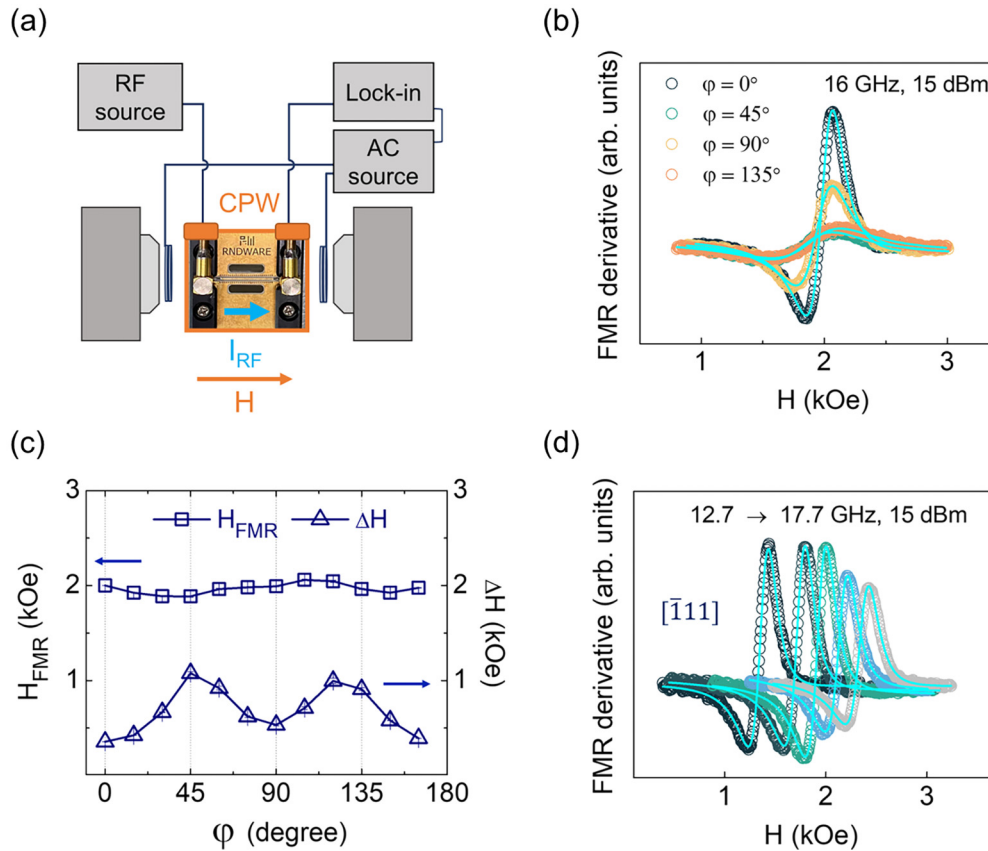
FIG. 2. (a) Schematic diagram of the broadband strip-line ferromagnetic resonance measurement system with the image of the coplanar waveguide (CPW) placed in the center of the electromagnet poles. The blue arrow represents the microwave current (I_{rf}) direction, and the orange arrow indicates the external magnetic field (H) direction. (b) The FMR derivative absorption signals of the Cr/Fe film with the in-plane magnetic field applied along $\varphi = 0°; 45°; 90°; 135°$. The I_{rf} was fixed at 16 GHz and 15 dBm. (c) Plot of resonance field (H_{FMR}) and linewidth (ΔH) as a function of φ. H_{FMR} and ΔH are deduced from FMR spectra fitted using Lorentzian function. (d) Frequency dependence of the FMR derivative spectra along [−111] crystal direction measured in the range 12.7–17.7 GHz.

dislocations, the crystal is still subjected to a small tensile strain, which explicitly explains the elongated peak in the RSM image. Besides, the TEM image also reveals that the Cr layer was grown following Volmer-Weber mode (island growth mode). The subsequent Fe layer was coherently grown on a Cr layer due to an excellent lattice match between Cr and Fe (∼0.6%), subsequently resulting in the orange-peel-like surface of the Fe layer. Such type of surface structure may affect the magnetocrystalline anisotropy of our film.

The film morphology was characterized using atomic force microscopy (AFM). An AFM image at a randomly selected location on the film surface, employing a scan size of 1 μm × 1 μm, as shown in Fig. 1(d). The analysis revealed that the estimated average roughness over a substantial area of 1 μm² is approximately 0.5 nm. We note that the thin film is homogeneous and continuous (see the Supplemental Material [20]), indicating the orientation independence of the grain distribution, which is a critical observation for understanding the film properties.

We characterized magnetic properties of our film using a vibrating sample magnetometer (VSM) [see Figs. 1(e) and 1(f)]. The azimuthal angle labeled by φ is defined as the angle between external magnetic field H and the [−111] crystal direction [inset of Fig. 1(f)]. The hysteresis loops were

collected by measuring magnetizing curves along different in-plane magnetic field angles (φ). From the hysteresis loops, we calculated the ratio of the remanence (M_r) to the saturation magnetization (M_s) as a function of φ, as summarized in Fig. 1(f). The estimated M_r/M_s ratio was found to be nearly angle independent, indicating a negligible magnetocrystalline anisotropy. Unlike the uniaxial magnetic anisotropy previously observed in the Cr/Fe bilayers [21], the observed isotropic behavior of the Cr/Fe (211) film in the present study is attributed to the large surface roughness.

The angular dependent FMR was obtained with the sample mounted on the coplanar waveguide surface under a DC magnetic field, as illustrated in Fig. 2(a). Figure 2(b) shows the typical derivatives of FMR taken at four different φ at 16 GHz. The observed FMR spectra were fitted using the Lorentzian function [22]. Based on the fits, the resonance field (H_{FMR}) and linewidth (ΔH) at a given rf were extracted accordingly. Figure 2(c) shows the dependence of H_{FMR} and ΔH on φ at every 15°. We observed that the H_{FMR} is independent of φ while ΔH exhibits a noticeable dependence on φ. The φ-independent H_{FMR} is attributed to the magnetic isotropy behavior, as shown in Fig. 1(f). On the other hand, the ΔH shows a strong anisotropy with respect to the angles φ. If a ferromagnetic film has a large uniaxial magnetic anisotropy
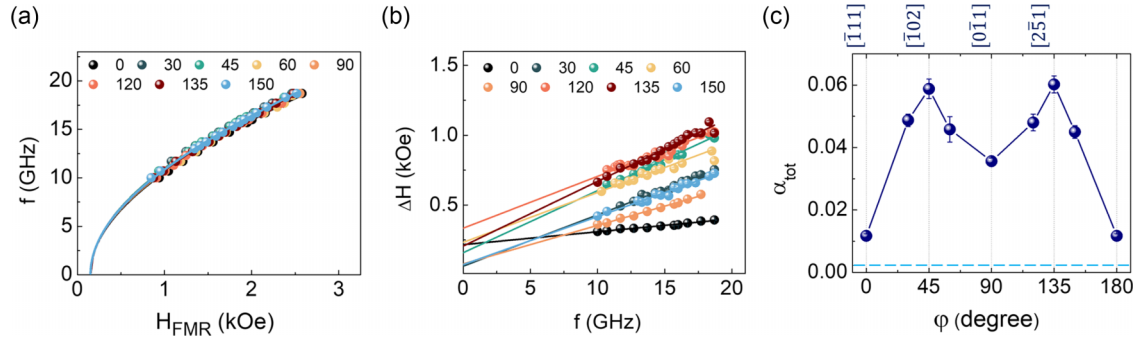
FIG. 3. (a), (b) Frequency dependence of resonance field (H_{FMR}) and linewidth (ΔH), respectively, at various in-plane φ angles. Solid lines are fitted curves using Eq. (1) (a) and Eq. (3) (b). The total magnetic damping (α_{tot}) are extracted from the slope of the Eq. (3) fitting. (c) Angular dependence of the α_{tot} in the Cr/Fe bilayer. The solid lines are guides for eyes. The dash line indicates the reference value of the magnetic damping of Fe given in Ref. [29]. Error bars are smaller than the symbol size.

and/or a large fourfold MCA, the magnetization of the film is hard to align to the hard-axis direction, thus resulting in the linewidth broadening in the FMR absorption spectra. This effect is known as the magnetic dragging effect and has been reported in previous literature [7,23]. However, this is not the case for our Cr/Fe film because of a nearly zero in-plane magnetic anisotropy, and all the resonances occurred in the magnetic field range over 500 Oe, where the magnetization is fully saturated. Therefore, this result is not related to the contribution of the dragging effect. Specifically, ΔH values reveal minima at $\varphi \sim 0°$, $90°$, and $\varphi \sim 180°$ and maxima at $\varphi \sim 45°$ and $\varphi \sim 135°$, meaning that magnetic damping of the Cr/Fe film could hold fourfold symmetry. Therefore, we conducted the frequency dependent FMR to accurately extract the α_{tot} in our bilayer. Figure 2(d) displays the frequency dependence of FMR derivative spectra measured in the range 12.7–17.7 GHz. The DC magnetic field (H) was swept along the Cr/Fe [−111] direction ($\varphi = 0°$). A frequency dependence experiment was also conducted along various azimuthal angles at every 15°. The deduced H_{FMR} and ΔH values were plotted in Fig. 3.

Figures 3(a) and 3(b) show the plot of the resonance frequency (f) against the resonance field (H_{FMR}) and the plot of the linewidth (ΔH) against the resonance frequency (f), respectively, at various in-plane φ angles labeled by colored solid circles. In the absence of in-plane magnetic anisotropy, the relation between resonance frequency f (GHz) and resonance field H_{FMR} (Oe) can be well fitted using the Kittel equation below [24]:

$$2\pi f = \gamma \sqrt{(H_{\text{FMR}} - H_{\text{a}})(H_{\text{FMR}} - H_{\text{a}} + 4\pi M_{\text{s}})}, \qquad (1)$$

where γ is the gyromagnetic ratio. H_{a} and M_{s} are the anisotropy field and saturation magnetization, respectively, and both were experimentally obtained from the VSM result. The parameter γ achieved from the fit was then used in the fitting of the relation between ΔH and f in Fig. 3(b) to extract the total damping α_{tot} in our sample.

Given that ΔH is the sum of many possible contributions, as follows:

$$\Delta H = \Delta H_0 + \Delta H_{\text{G}} + \Delta H_{\text{sp}} + \Delta H_{\text{TMS}}. \qquad (2)$$

ΔH_0 is a frequency-independent term originated from the inhomogeneity of the sample. ΔH_{G} contributed by Gilbert damping is an intrinsic character of the FM material.

Meanwhile, ΔH_{sp} represents the linewidth broadening due to the spin pumping from the FM to the adjacent NM layer, which is induced by the ferromagnetic resonance [25]. The last term, ΔH_{TMS}, is the linewidth broadening originated from the relaxation process called two-magnon scattering [26], which initiates by bulk and/or surface defects in the FM layer. Note that the second and the third terms in Eq. (2) linearly depend on the frequency while the fourth is a nonlinear function of frequency. However, such nonlinear behavior is only observed in high frequency range with approximately few tens' of GHz [26,27]. Figure 3(b) shows the deduced ΔH values plotted as a function of frequency (f). We can observe that ΔH scales linearly with f and the slopes of $\Delta H(f)$ differ greatly between in-plane angles. Our experimental data were fitted using the function below [28]:

$$\Delta H = \Delta H_0 + \frac{4\pi \alpha_{\text{tot}} f}{\gamma}. \qquad (3)$$

Here α_{tot} is the total magnetic damping of our Cr/Fe bilayer, which is the sum of all contribution from intrinsic (α_{G}) and other extrinsic (α_{TMS} and α_{sp}) effects as mentioned above. The parameters obtained from the best fits using Eqs. (1) and (3) are listed in Table I. The α_{tot} extracted from the slope of $\Delta H(f)$ function at different φ was shown in Fig. 3(c). The magnetic damping in our Cr/Fe bilayer shows strong angular dependence. Particularly, α_{tot} values vary from $\sim$0.012 along the [−111] direction to $\sim$0.060 near the [2−51] direction, which yields an anisotropy ($\Delta\alpha/\alpha_{\text{min}}$) of $\sim$400%. This large in-plane anisotropy of α_{tot} raises a relevant issue on which the relaxation channel would be the most dominant in our sample. To further clarify the possible mechanism accounting for the damping anisotropy, we conducted additional experiments, which will be discussed in the next section.

According to previous literature, the anisotropic α_{tot} originates from either intrinsic or extrinsic effects, as discussed in the following paragraphs.

Early theoretical work has provided a quantitative description of intrinsic magnetic damping in metallic ferromagnets using the breathing Fermi-surface model [29]. According to these studies, the Gilbert damping of a transition metallic ferromagnet is described by $\alpha_{\text{G}} \sim \xi^2 n(E_{\text{F}})$, where ξ is the strength of spin-orbit coupling (SOC), and $n(E_{\text{F}})$ is the density of state at Fermi level. Chen *et al.* [7] applied such a theory

TABLE I. Results for the fitting using Eqs. (1) and (3) for various in-plane φ angles: gyromagnetic ratio (γ), the inhomogeneous line broadening (ΔH_0), and the total magnetic damping (α). The saturation magnetization ($4\pi M_s$) of ~19405 Oe and the anisotropy field (H_a) of ~300 Oe were experimentally determined from the MH loops of the Cr/Fe film. The fitting errors were estimated using the least square method.

Parameter	0°	30°	45°	60°	90°	120°	135°	150°
γ (GHz/Oe)	$0.016 \pm 3.7 \times 10^{-5}$	$0.017 \pm 2.3 \times 10^{-5}$	$0.017 \pm 2.2 \times 10^{-5}$	$0.016 \pm 3.4 \times 10^{-5}$	$0.016 \pm 3.2 \times 10^{-5}$	$0.016 \pm 2.4 \times 10^{-5}$	$0.016 \pm 2.7 \times 10^{-5}$	$0.016 \pm 2.4 \times 10^{-5}$
ΔH_0 (Oe)	216 ± 7.42	62 ± 22.99	159 ± 35.28	233 ± 45.32	79 ± 10.83	334 ± 30.82	206 ± 31.65	73 ± 23.75
α	0.012 ± 0.0006	0.049 ± 0.0020	0.059 ± 0.0031	0.046 ± 0.0041	0.036 ± 0.0010	0.048 ± 0.0027	0.060 ± 0.0027	0.045 ± 0.0021

to explain the anisotropy of α_G in an epitaxially grown Fe on a GaAs substrate, where the twofold symmetry of interfacial SOC results in an anisotropic density of states at the interface of Fe and GaAs. Similarly, Li *et al.* found that the variation of SOC for different magnetization directions is responsible for damping anisotropy in an epitaxial binary alloy of Fe and Co. Interestingly, Li *et al.* observed that the angular dependence of α_G and anisotropic magnetoresistance (AMR) is coincident, since both phenomena originate from SOC [8]. In other words, damping anisotropy due to asymmetry in SOC should be reflected in the angular dependence of AMR.

In our case, weak magnetocrystalline anisotropy, which also relates to SOC, may imply that the variation of SOC with respect to the azimuthal angles is negligible. To confirm this assumption, we also conducted AMR measurement for our Cr/Fe bilayer along three in-plane angles $\varphi = 0°$, $45°$, and $90°$. Measurement configuration is schematically shown in Fig. 4(a), the longitudinal resistance along the x axis is measured while rotating the external magnetic field in the xz plane. The collected AMR data are presented in Fig. 4(b) with solid symbols in the upper part. The AMR ratio was calculated using the equation AMR (%) = $(R_{xz} - R_0)/R_0$ and summarized in Fig. 4(c) (solid circles). We found that the AMR results in our sample slightly vary with in-plane angles, which does not follow the α_{tot} trend. Moreover, the observed damping constant in our sample (approximately in the order of 10^{-2}) is significantly higher than the intrinsic damping reported earlier for Fe (in the order of $10^{-4} - 10^{-3}$) [30] as shown by the blue dashed line in Fig. 3(c). Therefore, we conclude that the intrinsic Gilbert damping does not provide a dominant contribution to the total magnetic damping of our Cr/Fe sample, hence other extrinsic effects should be considered.

One of the important extrinsic effects involved in the magnetic relaxation process in the FM/NM bilayer is the spin-pumping effect. In principle, the spin current induced by the magnetization precession in the FM layer is pumped into the adjacent NM layer, carrying away angular momentum to the NM layer. Consequently, this process provides an additional channel for spin dissipation, known also as non-local damping. According to spin-pumping theory, the magnitude of this effect is strongly affected by the transmission of the spin current through the FM/NM interface, which is parametrized by the spin mixing conductance ($g^{\uparrow\downarrow}$) [25]. The anisotropy of nonlocal magnetic damping is associated with the variation of the spin mixing conductance with respect to the φ. Since it is not possible to quantitatively separate the spin-pumping contribution from the total magnetic damping in this study, we intentionally investigated the angular dependence of another spin-related phenomenon, i.e., spin Hall magnetoresistance (SMR), as an alternative measurement as the spin-mixing conductance also plays a crucial role in SMR: the spin current is generated via the spin Hall effect in a NM then flows through the FM/NM interface into the neighboring FM layer, where it interacts with the magnetization and causes a resistance change, known as the SMR signal [31]. As in the spin pumping effect, the spin-mixing conductance is a key parameter for the strength of SMR. A higher spin-mixing conductance leads to a stronger spin current injection, thus resulting in a greater SMR signal. Investigating the angular
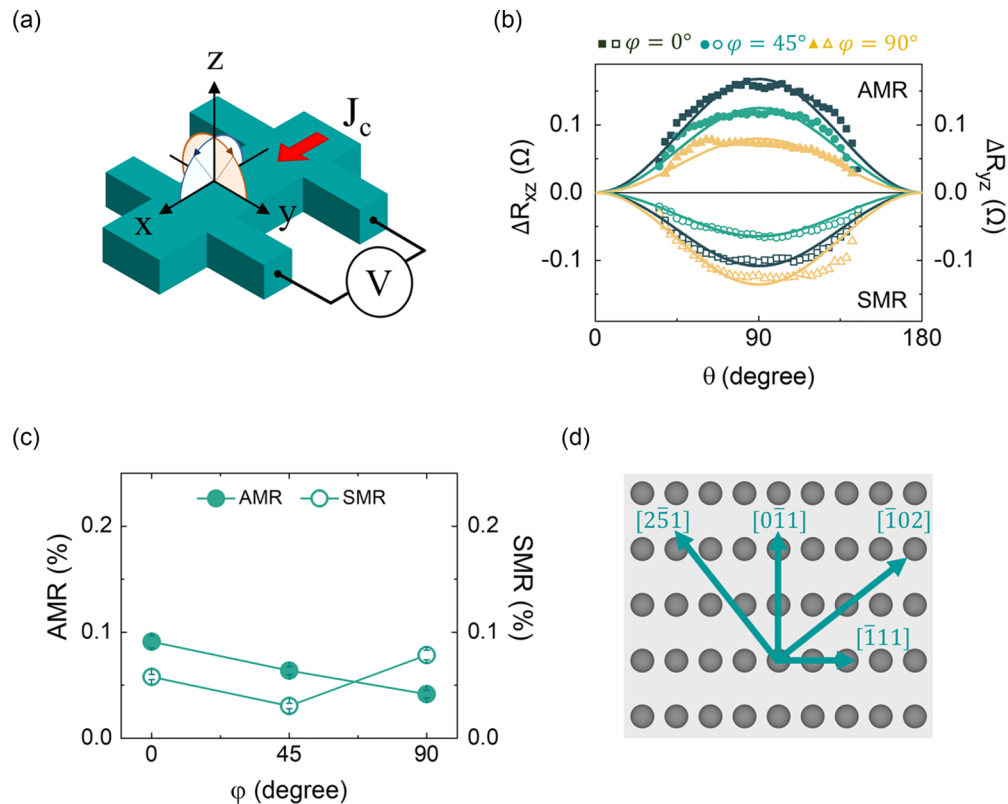
FIG. 4. (a) Schematic diagram of the Hall bar device and the measurement configurations of the anisotropic magnetoresistance (AMR) and the spin Hall magnetoresistance (SMR). The red arrow indicates the charge current (J_c) direction. The polar angle θ is defined by the angle between the external magnetic field and the normal direction of the film (z axis). (b) AMR data (solid symbols in the upper part) and SMR data (open symbols in the lower part) measured with the Hall bar devices along different in-plane angles ($\varphi = 0°$; 45°; 90°). The solid lines are fitting curves using $\sin^2(\theta)$ function. (c) Summary of AMR (solid symbols) and SMR (open symbols) results as a function of φ. Error bars are smaller than the symbol size. (d) Schematic of the Cr atomic arrangement from the top view of Cr (211) plane. The gray symbols represent Cr atoms. The blue arrows indicate crystal directions.

dependence of the SMR signal can provide valuable information on the variation of spin-mixing conductance with respect to in-plane angles, which, in turn, helps us to understand the in-plane anisotropy of the spin pumping effect in our Cr/Fe bilayer.

The measurement configuration is schematically shown in Fig. 4(a), where the longitudinal resistance along the x axis is measured while the external magnetic field is rotated in the yz plane. The SMR data are shown in Fig. 4(b) (open symbols in the lower part). The SMR ratio was then calculated using the equation SMR (%) = $(R_{yz} - R_0)/R_0$ and summarized in Fig. 4(c) (open circles). The observed SMR shows a different angular dependence, where the maximum occurs near $\varphi = 45°$. This result clearly indicates that the pronounced anisotropy of the magnetic damping in our Cr/Fe bilayer cannot be solely explained by the nonlocal damping contribution from spin pumping.

In addition to the spin pumping contribution, a process known as two-magnon scattering (TMS) is commonly considered. TMS involves the degeneration of the uniform precession mode ($k = 0$) into spin wave modes with ($k \neq 0$); here k is the wave vector determined by the magnon dispersion relation. In the theory [10,32,33], TMS is initiated at defect sites where the translation symmetry of crystal breaks, resulting in the nonconservation of the k vector. In general, the

presence of structural defects does not cause angle-dependent behavior if they are randomly distributed in the film plane. However, TMS is invoked to explain the fourfold symmetry of magnetic damping in some systems with crystal structure of cubic or tetragonal symmetry. To relax the strain induced by the lattice mismatch between materials in epitaxial thin films, structural defects such as dislocations are often introduced along the main crystallographic orientations which are also edges of the tetragonal structure. For this reason, α_{TMS} originated from these networks of dislocations would also follow the crystal symmetry, thereby reflecting twofold or fourfold anisotropy [11,34].

The Cr/Fe (211) bilayer in our study exhibits a tetragonal nature, where the two main crystal directions of the in-plane rectangular lattice are [−111] and [0−11], as schematically shown in Fig. 4(d). In fact, as shown in Fig. 1(c), arrays of dislocations formed along the [−111] direction due to an extremely large lattice mismatch of ∼17% compared to the [0−11] crystal direction (∼4%). It is expected that this crystal directions would have a large α_{TMS}. However, our observations show that the damping along this direction is at a minimum (∼0.012), while the maxima occur near the [−102] and [2−51] directions, which are diagonals of the rectangular lattice. Therefore, the two-magnon scattering model cannot adequately explain our observations.

An intriguing possibility is that the observed magnetic damping anisotropy in our bilayer could be attributed to the atomic arrangement within the in-plane film. Specifically, it is possible that the orbital texture is different with respect to the in-plane angles, leading to an angular-dependent behavior in the magnetic relaxation process. Recent studies have suggested that orbital ordering can play a significant role in the magnetic properties of a FM/$3d$-NM bilayer [16,35–37]. Further experimental and theoretical investigations are needed to elucidate the role of orbital ordering in the observed damping symmetry and to fully understand the complex interplay between intrinsic and several extrinsic damping mechanisms in magnetic thin films.

In conclusion, we experimentally investigated the angular dependence of α_{tot} in the epitaxial Cr/Fe bilayer. H_{FMR} was observed to be isotropic due to its negligible magnetocrystalline anisotropy, while ΔH was found to be highly anisotropic with fourfold symmetry. The extracted α_{tot} exhibited a strong angular dependence with up to ∼400% variation.

We found that the two representative extrinsic effects, spin pumping and two-magnon scattering, cannot explain our observation. One possible origin of our observation can be the angular momentum dissipation with the orbital nature in the Cr/Fe bilayer, which strongly depends on crystallographic orientation. Our results provide insights into the anisotropic nature of α_{tot} in bilayer systems composed of a ferromagnet and a $3d$ nonmagnetic metal that must be taken into consideration in the designs of spintronic devices.

[1] H. Yu, O. d'Allivy Kelly, V. Cros, R. Bernard, P. Bortolotti, A. Anane, F. Brandl, R. Huber, I. Stasinopoulos, and D. Grundler, Sci. Rep. **4**, 6848 (2014).

[2] A. J. Lee, J. T. Brangham, Y. Cheng, S. P. White, W. T. Ruane, B. D. Esser, D. W. McComb, P. C. Hammel, and F. Yang, Nat. Commun. **8**, 234 (2017).

[3] J. H. Moon, T. Y. Lee, and C.-Y. You, Sci. Rep. **8**, 13288 (2018).

[4] G. E. Rowlands, C. A. Ryan, L. Ye, L. Rehm, D. Pinna, A. D. Kent, and T. A. Ohki, Sci. Rep. **9**, 803 (2019).

[5] J. Seib, D. Steiauf, and M. Fähnle, Phys. Rev. B **79**, 092418 (2009).

[6] K. Gilmore, M. D. Stiles, J. Seib, D. Steiauf, and M. Fähnle, Phys. Rev. B **81**, 174414 (2010).

[7] L. Chen, S. Mankovsky, S. Wimmer, M. A. W. Schoen, H. S. Körner, M. Kronseder, D. Schuh, D. Bougeard, H. Ebert, D. Weiss, and C. H. Back, Nat. Phys. **14**, 490 (2018).

[8] Y. Li, F. Zeng, S. S.-L. Zhang, H. Shin, H. Saglam, V. Karakas, O. Ozatay, J. E. Pearson, O. G. Heinonen, Y. Wu, A. Hoffmann, and W. Zhang, Phys. Rev. Lett. **122**, 117203 (2019).

[9] A. A. Baker, A. I. Figueroa, C. J. Love, S. A. Cavill, T. Hesjedal, and G. van der Laan, Phys. Rev. Lett. **116**, 047201 (2016).

[10] J. Lindner, K. Lenz, E. Kosubek, K. Baberschke, D. Spoddig, R. Meckenstock, J. Pelzl, Z. Frait, and D. L. Mills, Phys. Rev. B **68**, 060102(R) (2003).

[11] G. Woltersdorf and B. Heinrich, Phys. Rev. B **69**, 184417 (2004).

[12] E. E. Fullerton, M. J. Conover, J. E. Mattson, C. H. Sowers, and S. D. Bader, Phys. Rev. B **48**, 15755 (1993).

[13] C. D. Potter, R. Schad, P. Belien, G. Verbanck, V. V. Moshchalkov, Y. Bruynseraede, M. Schäfer, R. Schäfer, and P. Grünberg, Phys. Rev. B **49**, 16055(R) (1994).

[14] M. D. Stiles, Phys. Rev. B **54**, 14679 (1996).

[15] M. Velez and I. K. Schuller, J. Magn. Magn. Mater. **184**, 275 (1998).

[16] D. Jo, D. Go, and H.-W. Lee, Phys. Rev. B **98**, 214405 (2018).

[17] G. Sala and P. Gambardella, Phys. Rev. Res. **4**, 033037 (2022).

[18] J. Zhang, H. Xie, X. Zhang, Z. Yan, Y. Zhai, J. Chi, H. Xu, Y. Zuo, and L. Xi, Appl. Phys. Lett. **121**, 172405 (2022).

[19] K. Serizawa, M. Ohtake, T. Kawai, M. Futamoto, F. Kirino, and N. Inaba, J. Magn. Magn. Mater. **477**, 420 (2019).

[20] See Supplemental Material at http://link.aps.org/supplemental/10.1103/PhysRevMaterials.8.L041401 for details of the growth, crystal structure, surface morphology, and the magnetic properties of the Cr/Fe bilayers.

[21] T.-H. T. Nguyen, V. Q. Nguyen, S. Jeong, E. Park, H. Jang, N. J. Lee, S. Lee, B.-G. Park, S. Cho, H.-W. Lee, J.-I. Hong, and S. Kim, Commun. Phys. **4**, 247 (2021).

[22] J. Park, I. Oh, A.-Y. Lee, H. Jang, J.-W. Yoo, Y. Jo, and S.-Y. Park, J. Alloys Compd. **829**, 154534 (2020).

[23] Y. Li, Y. Li, Q. Liu, Z. K. Xie, E. Vetter, Z. Yuan, W. He, H. L. Liu, D. L. Sun, K. Xia, W. Yu, Y. B. Sun, J. J. Zhao, X. Q. Zhang, and Z. H. Cheng, New J. Phys. **21**, 103040 (2019).

[24] A. Conca, S. Keller, L. Mihalceanu, T. Kehagias, G. P. Dimitrakopulos, B. Hillebrands, and E. T. Papaioannou, Phys. Rev. B **93**, 134405 (2016).

[25] Y. Tserkovnyak, A. Brataas, and G. E. W. Bauer, Phys. Rev. B **66**, 224403 (2002).

[26] K. Lenz, H. Wende, W. Kuch, K. Baberschke, K. Nagy, and A. Jánossy, Phys. Rev. B **73**, 144424 (2006).

[27] Kh. Zakeri, J. Lindner, I. Barsukov, R. Meckenstock, M. Farle, U. von Hörsten, H. Wende, W. Keune, J. Rocker, S. S. Kalarickal, K. Lenz, W. Kuch, K. Baberschke, and Z. Frait, Phys. Rev. B **76**, 104416 (2007).

[28] S. Sakamoto, T. Higo, S. Tamaru, H. Kubota, K. Yakushiji, S. Nakatsuji, and S. Miwa, Phys. Rev. B **103**, 165122 (2021).

[29] V. Kamberský, Can. J. Phys. **48**, 2906 (1970).

[30] S. Wu, D. A. Smith, P. Nakarmi, A. Rai, M. Clavel, M. K. Hudait, J. Zhao, F. M. Michel, C. Mewes, T. Mewes, and S. Emori, Phys. Rev. B **105**, 174408 (2022).

[31] J. Kim, P. Sheng, S. Takahashi, S. Mitani, and M. Hayashi, Phys. Rev. Lett. **116**, 097201 (2016).

[32] M. J. Hurben and C. E. Patton, J. Appl. Phys. **83**, 4344 (1998).

[33] R. Arias and D. L. Mills, Phys. Rev. B **60**, 7395 (1999).

[34] Y. Zhang, G. Wu, Z. Ji, S. Zhou, H. Xue, Z. Li, S. Zhang, J. Zhang, Y. Liu, Q. Jin, and Z. Zhang, ACS Appl. Mater. Interfaces **14**, 24039 (2022).

[35] D. Go and H.-W. Lee, Phys. Rev. Res. **2**, 013177 (2020).

[36] S. Lee, M.-G. Kang, D. Go, D. Kim, J.-H. Kang, T. Lee, G.-H. Lee, J. Kang, N. J. Lee, Y. Mokrousov, S. Kim, K.-J. Kim, K.-J. Lee, and B.-G. Park, Commun. Phys. **4**, 234 (2021).

[37] H. C. Lyu, Y. C. Zhao, J. Qi, G. Yang, W. D. Qin, B. K. Shao, Y. Zhang, C. Q. Hu, K. Wang, Q. Q. Zhang, J. Y. Zhang, T. Zhu, Y. W. Long, H. X. Wei, B. G. Shen, and S. G. Wang, J. Appl. Phys. **132**, 013901 (2022).